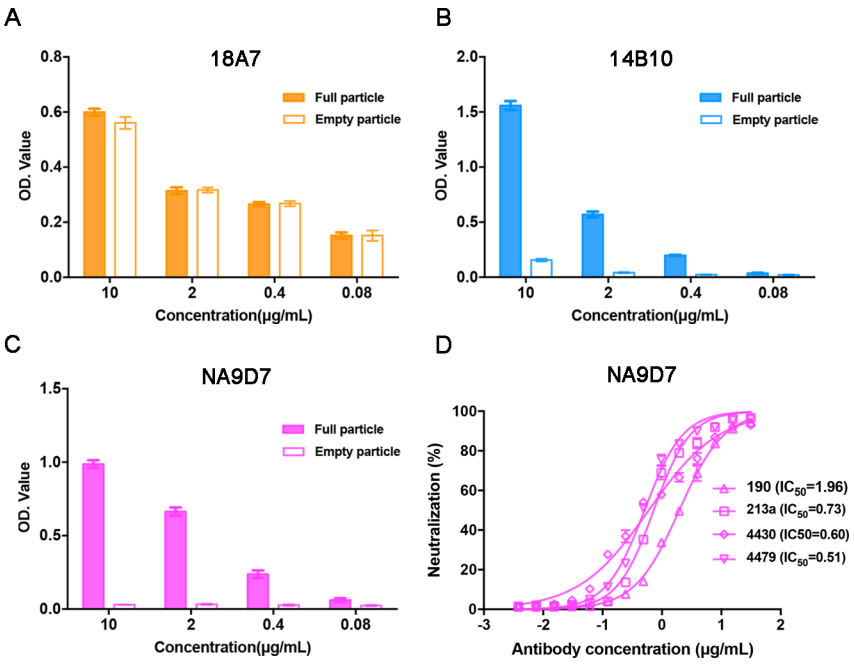

Figure S1. Characterization of the 18A7, 14B10 and NA9D7neutralization antibodies, Related to Figure 1.

(A-C) Binding efficiencies of the neutralizing antibodies 18A7 (A), 14B10 (B) and NA9D7 (C) to CVA16 full particle or empty particle, as evaluated by binding ELISA. Values are expressed as mean ± s.d.

(D) Cross-neutralizing efficacy of NA9D7 against CVA16 strains 190, 213a, 4430, and 4479 were evaluated by an *in vitro* micro-neutralization assay in human rhabdomyosarcoma (RD) cells, respectively.

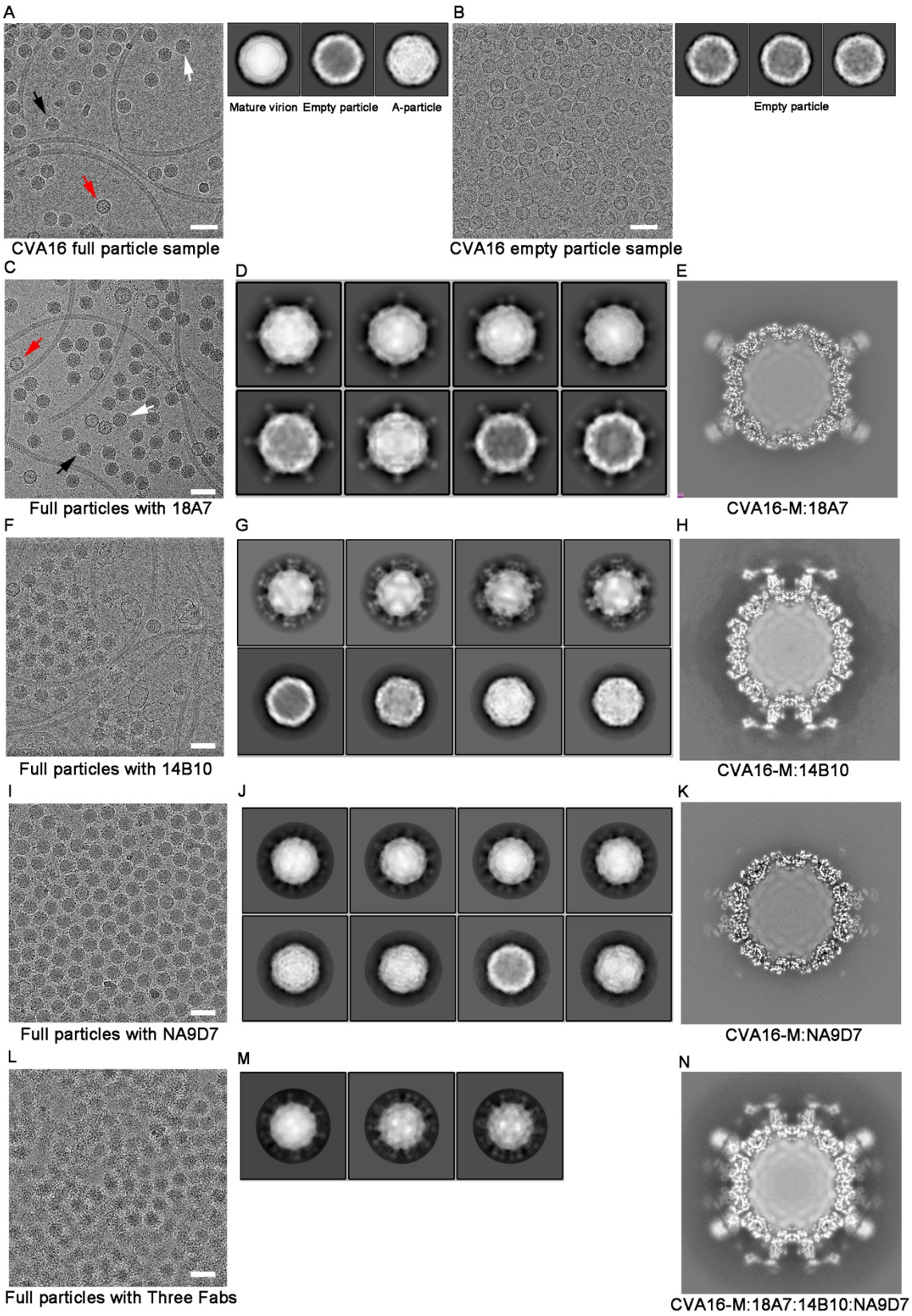

Figure S2. Raw cryo-EM images and structural determination of the three types of CVA16 particles and its immune complexes, Related to Figure 2 and Figure 4.

(A and B) Selected cryo-EM images (left) and corresponding representative 2D classes (right) of CVA16 full particle (A) and empty particle (B) samples.
(C-N) Selected cryo-EM images of CVA16-M:18A7 (C), CVA16-M:14B10 (F), CVA16-M:NA9D7 (I), and CVA16-M:18A7:14B10:NA9D7 (L). 2D classes (D, G, J, M) and central sections (E, H, K, N) of the corresponding CVA16 immune complexes. Scale bar, 50 nm. Black, white and red arrows indicate CVA16 mature virion, A-particle, and empty particle, respectively.

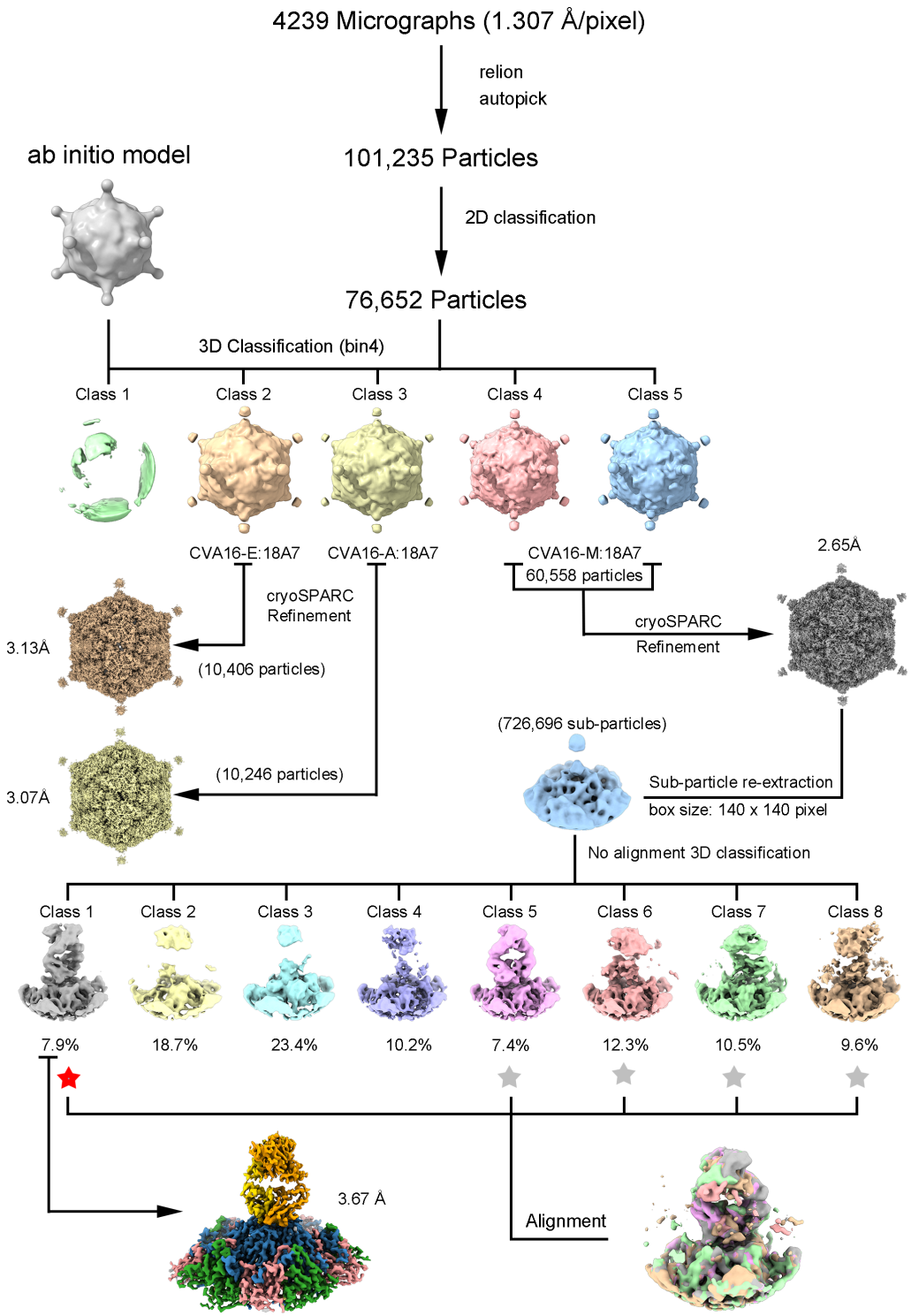

Figure S3. Flowchart of the localized reconstruction of CVA16:18A7 complexes, Related to Figure 2 and STAR Methods.

Step 1: Initial model generation, 3D classification and refinement when imposing icosahedral symmetry. Step 2: Localized reconstruction of the 5-fold region of CVA16-M:18A7, which finally yielded a map of 3.67-Å resolution. Please refer the Methods section for details.

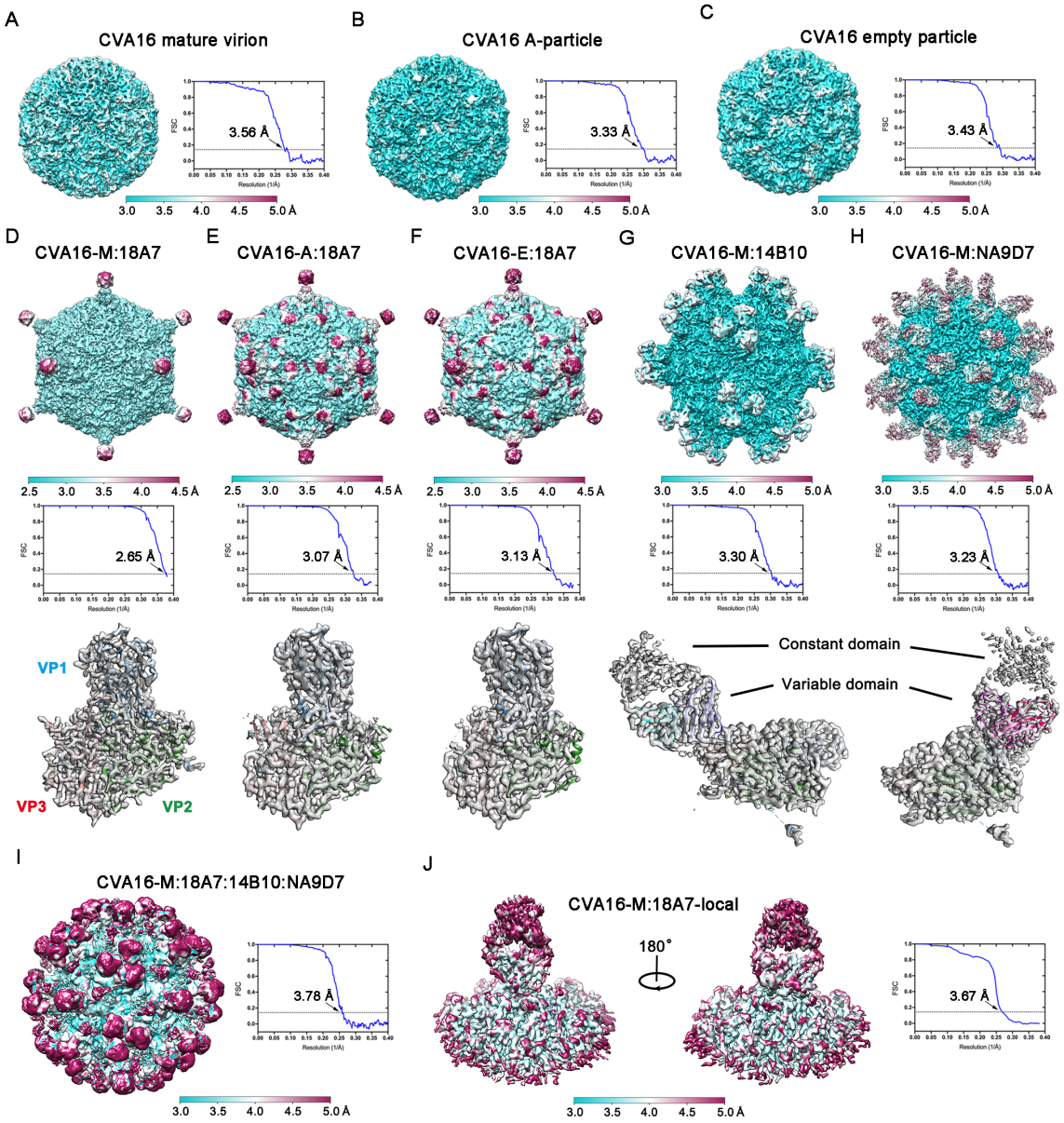

Figure S4. Local resolution and gold-standard Fourier Shell Correlation (FSC) plots for different particle types of CVA16 virus and the immune complexes, Related to Figure 2, Figure 4 and Table 1.
(A-C) The local resolution and FSC curves of CVA16 mature virion (A), CVA16 A-particle (B) and CVA16 empty virus (C).
(D-H) The local resolution, FSC curves and the segmented asymmetric units of CVA16-M:18A7 (D), CVA16-A:18A7 (E), CVA16-E:18A7 (F), CVA16-M:14B10 (G) and CVA16-M:NA9D7 (H). The segmented maps (gray) were fitted with the atomic models (ribbon diagrams) of the three or four capsid proteins and the Fab variable domain (VP1: light blue, VP2: light green, VP3: light red, VP4: light yellow; 14B10 heavy chain: cyan, 14B10 light chain: blue; NA9D7 light chain: red, NA9D7 heavy chain: magenta).
(I-J) The local resolution and FSC curves of CVA16-M:18A7:14B10:NA9D7 (I) and CVA16-M:18A7-local (J).

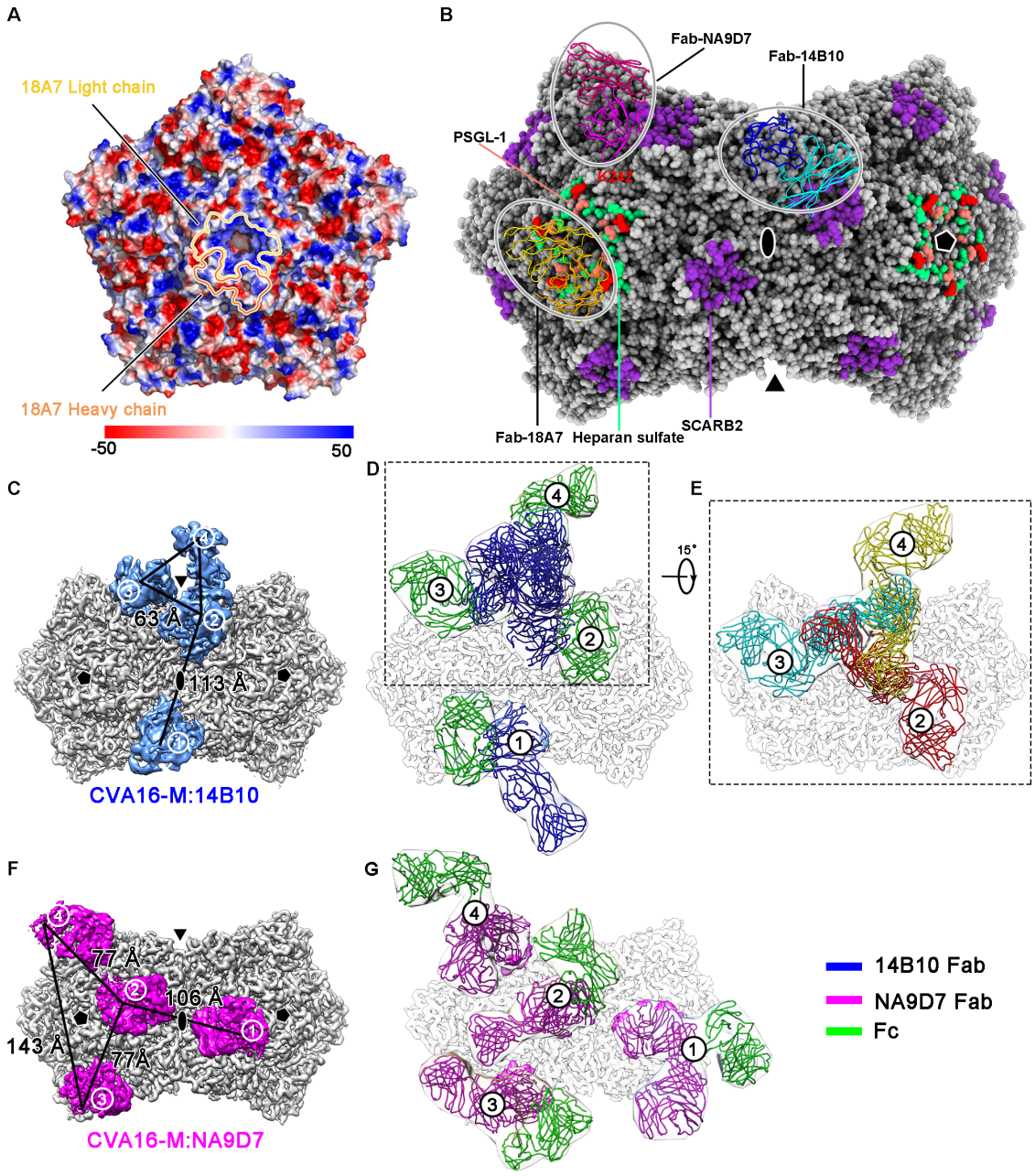

Figure S5. Epitope analysis of nAbs 18A7, 14B10, NA9D7, Related to Figure 3.

(A) Electrostatic surface potential rendering of the CVA16 pentamer. The scale bar refers to the electrostatic potential, ranging from −50 kTe^{-1} to +50 kTe^{-1} (red, negative; blue, positive; PyMol using APBS tools). The ellipse curves embrace the footprint of Fab 18A7 on the CVA16 mature virion (yellow, light chain; orange, heavy chain).

(B) Two pentamers of the CVA16 viral capsid are shown as spheres, Fab 18A7, 14B10, and NA9D7 are displayed in ribbon mode. The binding sites of known receptor SCARB2, PSGL-1, and heparan sulfate are colored purple, green, and orange respectively. Residue K242 of VP1 (red) is involved in PSGL-1 and heparan sulfate binding.

(C and F) Spatial relationship of four adjacent Fabs in the maps of both CVA16-M:14B10 (C) and CVA16-M:NA9D7 (E).

(D and G) Potential analysis of bivalent interaction for full-length antibodies 14B10 and NA9D7. The models of full-length antibodies (PDB no. 1IGY) were fitted to the representative Fab densities. If a

bivalent interaction is possibly occurring for a full-length antibody, two fitted full-length antibodies will overlap or nearly superimpose each other considering the hinge linking two Fabs highly flexible in an antibody. Obviously, no such instance is happening.
(E) Potential analysis of the steric hindrance for the binding of full-length antibody 14B10. Only one full-length antibody 14B10 could bind to one of the three sites around 3-fold axis and let the rest two sites unoccupied due to steric hindrance. By contrast, no steric hindrance is observed for the binding of full-length antibody NA9D7, see Figure S5G.

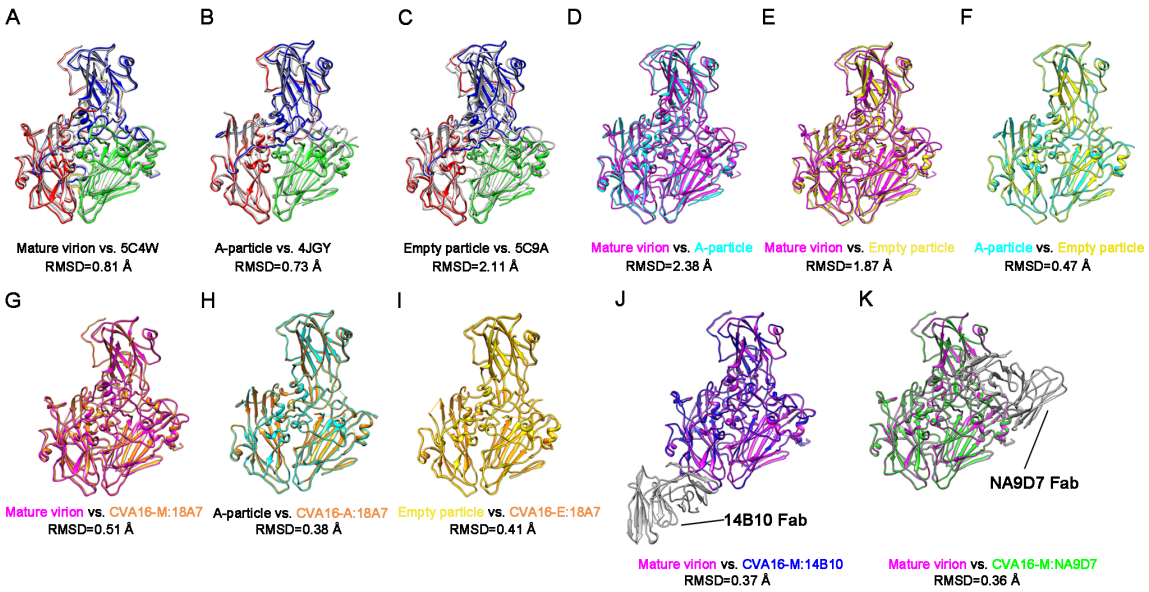

Figure S6. Superposition of the protomers between our CVA16 viral structures and previously reported structures or their immune complexes, Related to Figure 4.

(A-C) Superpositions of the protomers between our CVA16 viral structures and previously reported structures. The VP1, VP2, VP3, and VP4 regions of CVA16 mature virion (A), A-particle (B), empty particle (C) are blue, green, red, and yellow, respectively. The protomers of the reported CVA16 crystal structures are gray. The PDB (Protein Data Bank) codes are 5C4W, 4JGY and 5C9A, corresponding to the CVA16 mature virion, A-particle, empty virus, respectively.

(D-F) Superpositions of the protomers between mature virion (magenta) and A-particle (cyan) (D), mature virion and empty particle (yellow) (E), and A-particle and empty particle (F), respectively.

(G-I) Superpositions of the protomers of CVA16 viral structures with its corresponding 18A7 immune complexes (orange).

(J and K) Superpositions of the protomer of mature virion with CVA16-M:14B10 (blue) (J) and CVA16-M:NA9D7 (green) (K). The Fab 14B10 and NA9D7 were colored by gray. The RMSD values were calculated using the Chimera "MatchMaker" tool.